Laser Scanning Intensity Fingerprint: 3D Visualisation and Analysis of Building Surface Deficiencies

Daniel Antón, Manuel J. Carretero-Ayuso, Juan Moyano-Campos, and Juan E. Nieto-Julián

Abstract Terrestrial laser scanning (TLS) is a widely used technology in numerous sectors since it enables the recording of both geometric data and colour information of the objects. Moreover, this remote sensing technique allows for producing point clouds enhanced with the reflection intensity of the laser beam. Scientific research has used those data to detect and assess building surface deficiencies. However, the laser scanning intensity fingerprint of a building pathology is yet to be addressed. Thus, this research quantitatively analyses the distribution of point cloud intensities throughout the object geometry to show changes against the general context of the building component surface. This intensity fingerprint reveals the extent of the pathology, which leads to filtering the point cloud by those intensity values to extract and calculate the surface defect. On this basis, TLS is proven to be useful to record, detect, characterise, and examine specific building surface deficiencies and carry out the conservation status analysis of the assets surveyed. The case studies in this chapter are heritage buildings with clear surface pathologies. However, given the relationship between the building surface deficiencies and the point cloud data intensities, this research can also be applied to detect anomalies in modern buildings and constructions.

D. Antón (✉)
Research Group 'TEP970: Innovación Tecnológica, Sistemas de Modelado 3D y Diagnosis Energética en Patrimonio y Edificación', Departamento de Expresión Gráfica e Ingeniería en la Edificación, Escuela Técnica Superior de Ingeniería de Edificación, Universidad de Sevilla, 4A Reina Mercedes Avenue, 41012 Seville, Spain
e-mail: danton@us.es

Department of Product Design, School of Architecture, Design and the Built Environment, Nottingham Trent University, 50 Shakespeare Street, Nottingham NG1 4FQ, UK

M. J. Carretero-Ayuso
Departamento de Arquitectura, Universidad de Alcalá, 8 Santa Úrsula Street, 28801 Alcalá de Henares, Spain

J. Moyano-Campos · J. E. Nieto-Julián
Departamento de Expresión Gráfica e Ingeniería en la Edificación, Escuela Técnica Superior de Ingeniería de Edificación, Universidad de Sevilla, 4A Reina Mercedes Avenue, 41012 Seville, Spain

1   Introduction

Building pathologies are diverse in terms of their originating action, their type and
extent, and the characteristics of the materials used. These defects or anomalies, being
either of a physical–mechanical, chemical or biological nature or a combination of
them [23], can occur from the moment the buildings are erected. Not only do these
problems arise from the interaction of individual components but also due to the
interaction of the building with its occupiers and its environment, as well as because
of the exposure time [24]. Likewise, other factors such as malpractice in building
design, construction, and maintenance are also the cause of building pathologies [5].
As a consequence of their age, historic buildings and constructions are more likely
to present surface deficiencies, but modern buildings are not exempt from this.

In the scientific community, the use of massive data capture technologies [21]
has increased in the latest decades. These systems include terrestrial laser scan-
ning (TLS), the structure-from-motion (SfM) photogrammetric technique, mechan-
ical scanning sonar (MSS), infrared thermography (IRT), among others. Being also
intended for diverse purposes, remote sensing is used to and capable of recording the
deficiencies in a short time and with much more significant detail than using tradi-
tional methods. What is more, irregularities inherent to building deficiencies could
only be recorded by these means, which in turn enables the as-built modelling and
accurate analysis of the geometrical alterations of heritage assets [2, 3, 10]. In this
sense, Dias et al. [6] carried out a thorough analysis of the scientific literature on the
use of advanced digitisation techniques for the detection and diagnosis of building
anomalies. The authors concluded that, although these technologies help the visual
assessment building façades, there are still great efforts to make in terms of accuracy
and reliability in the analysis.

Previous research publications in the field have addressed the implementation of
TLS and unsupervised classification methods into the mapping of defects of historic
buildings via the study of point cloud intensities [4]. Having carried out the classifi-
cation of defects, Kim et al. [16] presented an automatic diagnosis approach based
on TLS for the localisation and quantification of concrete spalling on structures.
Masiero and Costantino [22] implemented statistical filtering and machine learning
to detect and calculate millimetric damages on brick surfaces of façades from TLS
point cloud data. Instead of using cloud intensities, the researchers focused on the
computation of distances between points of the brick damaged area and a refer-
ence plane on the façade surface. Also working on TLS data via machine learning,
Valero et al. [28] processed geometric and SfM colour data to automatically identify
and classify material loss defects and discolouration on ashlar structures. Suchocki
et al. [26] proposed a method to identify and validate construction surface defects by

using TLS radiometric data (laser intensity). The method was also useful to down-size point clouds via eliminating redundant information, which has an impact on both the computational efforts in processing large datasets and the conservation of spatial data of interest. However, subsampling the point clouds to such an extent (5%) implies that the total number of points affected by the pathology cannot be measured as in this research, nor the full pathology can be mapped. More related to the cataloguing of façade materials than to the analysis of building surface deficiencies, Lezzerini et al. [20] used TLS to record the masonry of the Italian St. Nicholas Church in Pisa. Next, using a Geographical Information System (GIS), these authors mapped the façade components with a view to providing essential information as regards their materials and construction techniques. On the other hand, Antón and Amaro-Mellado [1] highlighted the importance of the digital level (digital number, DN) of the images in the analysis of data. Instead of TLS, they focused on a different remote sensing data source, IRT, also called the infrared thermovision technique. Utilising a GIS and 3D point cloud data processing software, these researchers made use of the DN of the infrared images to produce 3D thermal data to represent the thermal behaviour of buildings and bodies.

In view of all the above, considering the capability of TLS to produce intensity data, the research objective is to explore the characterisation of building surface deficiencies through point cloud intensities. In other words, the aim is to analyse the laser scanning intensity fingerprint of building pathologies on surfaces for their detection and quantification.

This chapter is structured as follows: Firstly, the case studies are presented. Next, the Methodology section explains the approach, equipment, technologies, and processes considered. Following the discussion of the results achieved, the conclusions and future work take place.

2 Case Studies

This section briefly introduces the case studies through which the research objective will be fulfilled. In this chapter, the focus will be on sectors of building components or constructions with visible surface deficiencies caused by different agents. The description of each case study includes concise and diverse details of their history, features, surroundings, and current conservation status.

2.1 St. Andrew's with Castle Gate United Reformed Church, Nottingham

The formerly Presbyterian and now congregation called St. Andrew's with Castle Gate United Reformed Church [25], known as St. Andrew's with Castle Gate URC or

Fig. 1 Colour change in
northwest faces of buttresses

commonly and simply as St. Andrew's Church, is registered by the Charity Commission, with the attached former Sunday school, with number 1129944. This institution is based in Nottingham, United Kingdom, in a Grade II listed heritage building (List Entry Number: 1270832), dated 1869 [11]. This church in the Gothic Revival style is surrounded by a wall with railings, also Grade II listed (List Entry Number: 1247549) by Historic England [12]. The church is located opposite the western side of the main buildings of the City Campus of Nottingham Trent University.

In relation to the conservation status of the case study, as shown in Fig. 1, both the church's straight buttresses and the boundary wall evidence a change in the colour of the masonry work in comparison with other areas without this pathology or presenting minor surface deficiencies. In this way, the vertical plane of the buttress and the wall sector on the right (except for the window area) were considered for this research as the affected area and the reference zone for comparison, respectively.

2.2 Bromley House, Beeston, Nottingham

There are numerous buildings, elements, and parks and gardens, or parts of them, that have been listed by Historic England throughout the country since 1882. A search in the city of Nottingham alone returns 822 results for heritage assets [13]. It is the case of a residential building in the Victorian style called Bromley House, in

Fig. 2 Bromley House. Efflorescence on the lower part of the western wall. *Source* Google Street View [8]

Beeston, that was the former Board School that can be seen in Fig. 2. This building is located opposite the eastern side of St. John the Baptist Parish Church, also known as Beeston Parish Church, a mid-nineteenth-century Anglican church. This heritage building, listed as Grade II (List Entry Number: 1263823) [14], has undergone several restorations and extensions in the course of its history, such as those of the tower, the bells, the roofs, and the walls [27].

Regarding Bromley House, the building area incorporates the Village Cross, the shaft of the fourteenth-century cross of the village centre, a Grade II listed (List Entry Number: 1263870) heritage asset [15] that was re-erected there in 1929.

The part of Bromley House addressed in this research is the lower section of the ground floor western façade, which is made of traditional red brick. As a result of capillarity humidities, the façade shows efflorescence in diverse degrees, ranging from low-density areas to those with intense white stains, together with a slight loss of mass in some bricks.

3   Methodology

The recording and processing of remote sensing data of building surface deficiencies are described in this section. The materials and methods involved consist of the approach adopted in this research, together with the equipment, technologies, and processes implemented. Thus, this section is subdivided into two different stages, *Data collection*, and *Data processing*.

3.1 Data Collection

In this way, it is essential to describe the arrangement in the 3D surveys and the setting of parameters. In this subsection, the TLS equipment used to capture the geometry of the two case studies consisted of a tripod-mounted Leica ScanStation P20 [17] 3D laser scanner. The scanner positions (known as stations) and parameters set for each one will be indicated separately.

- *St. Andrew's Church*

  The resolution of the laser scanner was set to 3.1 mm at 10 m distance, and the 3D survey was configured as scan only (no images were taken). The number of points (horizontal × vertical) for that resolution was 20,107 × 8099. The scan quality was set to 3 out of 4. The 3D survey consisted of two scans. With a view to easing the overlap of scan data, the stations were placed 1.5 m apart at 5.5 and 6 m distance from the buttress vertical plane. Due to the proximity of the stations, no targets were used in the laser scanning. The scanning time was 27 min. The time to set the second station is not considered.

- *Bromley House*

  The resolution of the laser scanner was set to 3.1 mm at 10 m distance, and the 3D survey was configured as scan only (no images were taken). The number of points (horizontal × vertical) for that resolution was 20,107 × 8099. The scan quality was set to 3 out of 4. The 3D survey consisted of a single scan (no registration process was needed). The scanning time was 13 min and 30 s.

3.2 Data Processing

Once the geometric data were recorded, Leica Cyclone 9.4 software [18] was used to produce the case studies' point clouds. To do this, the scan data were imported into the application. As seen in Sect. 3.1, no images were recorded during the 3D surveys, which means that no textures had to be mapped onto the point clouds. This research analyses the laser beam intensities instead of RGB (red–green–blue) coloured textures. In addition, only the St. Andrew's Church case study required scan registration (alignment of scans into the same coordinate system) since it consisted of two stations. This was carried out automatically in the software by creating one cloud constraint, but the optimisation of the alignment was also conducted to minimise the group error.

Besides, it should be noted that the TLS data were recorded and produced in a local coordinate system for each case study. In other words, no geo-referencing process was performed. Given that the analysis carried out focuses on the geometry and the laser beam intensity data on surfaces, the geo-referencing of the point clouds would not make any difference to the results of this research.

After the point cloud data were produced and stored in *.e57* file format, these datasets were manually segmented to select the desired sector to be studied in each case. Using the open-source CloudCompare software [7], this was achieved by conducting manual polygon fencing in the elevation view (*XZ* plane orthogonal view). Thus, the undesired areas were eliminated to extract the segmented point clouds: the pathology sector (1) and the reference zone (2). In addition, the TLS data were subsampled at 20 mm resolution to try to homogenise the unordered datasets, thus reducing their information entropy [9].

The methodology of this research also involved various processes such as: enquiring the TLS data intensities; producing histograms of the distribution of points among intensity intervals; gathering statistical data from those histograms; filtering the segmented point clouds by laser beam intensity values to isolate the affected areas from the rest of the sectors; likewise, presenting the point cloud data intensities in different visualisation modes with a view to highlighting the affected areas. The processes above were also carried out in CloudCompare software.

4 Results and Discussion

This section is structured into two different subsections. Firstly, the outcomes deriving from the research objectives are presented and discussed. This involves showing the digitised areas of the case studies, carrying out the analysis of the TLS data and discussing the findings achieved. Secondly, the research limitations are described and included in a separate subsection.

Prior to addressing this section, it is worth providing the main specifications of the computer used to process the data. It was a gaming laptop of the latest generation with an octa-core processor with hyper-threading at 2.30 GHz and a maximum turbo frequency of 4.60 GHz with 24 MB cache, 32 GB RAM DDR4 @ 3200 MHz, a 192-bit graphics card with 3840 cores @ 1425 MHz and 6144 MB GDDR6 dedicated memory @ 14 Gbps, and an NVMe PCIe Gen3x4 SSD (solid-state drive) with 1 TB storage capacity.

4.1 Laser Beam Intensity Fingerprint

The research objective is to analyse the intensities of point clouds so that building surface deficiencies can be characterised. Given that the reflection of the laser beam varies depending on the surface colour, material, texture, and humidity content, the buttress of St. Andrew's Church and the lower wall sector of Bromley House are suitable case studies to reveal the laser beam intensity fingerprint since they present surface deficiencies.

4.1.1   St. Andrew's with Castle Gate URC

As mentioned before, the change in the buttress colour can be recorded using TLS and next producing the point cloud data enhanced with intensities. Firstly, it is worth specifying the registration diagnostics of the two scans of the St. Andrew's Church case study:

- Mean absolute error for enabled constraints: 0.001 m
- Overlap point count: 100,266 points
- Overlap error statistics:

  – RMS (Root Mean Square) error: 0.0100678 m
  – Average: 0.00559179 m
  – Minimum: 1.04814e−06 m
  – Maximum: 0.0908525 m.

Based on both the above data and the validity of the alignment, the next step was to use CloudCompare software to enquire the intensity values from the segmented point clouds: (1) pathology sector and (2) reference zone.
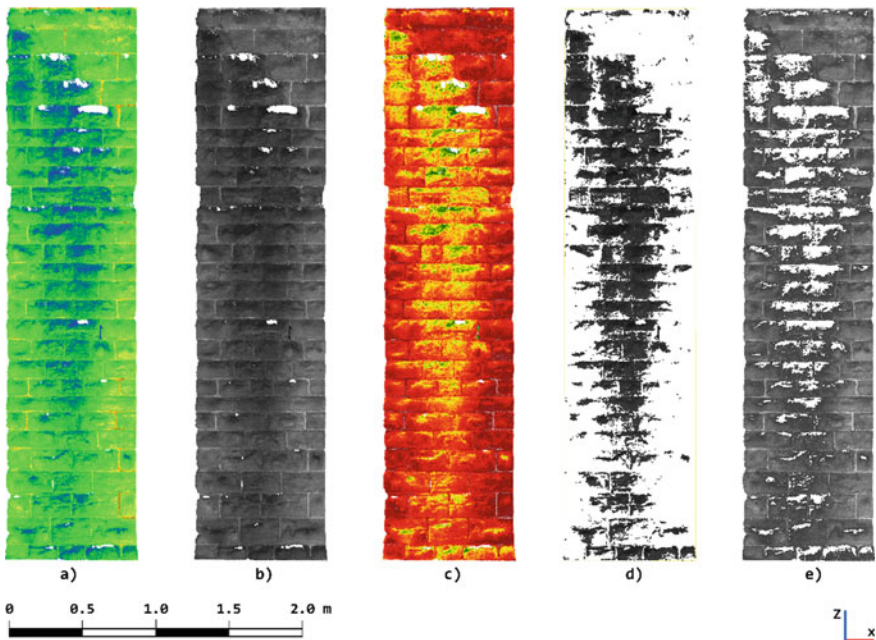
Fig. 3 Segmented pathology buttress sector enhanced with intensities: **a** blue–green–yellow–red; **b** greyscale (monochrome); **c** high contrast; **d** most severely affected part, in monochrome; **e** the rest of the sector, in monochrome
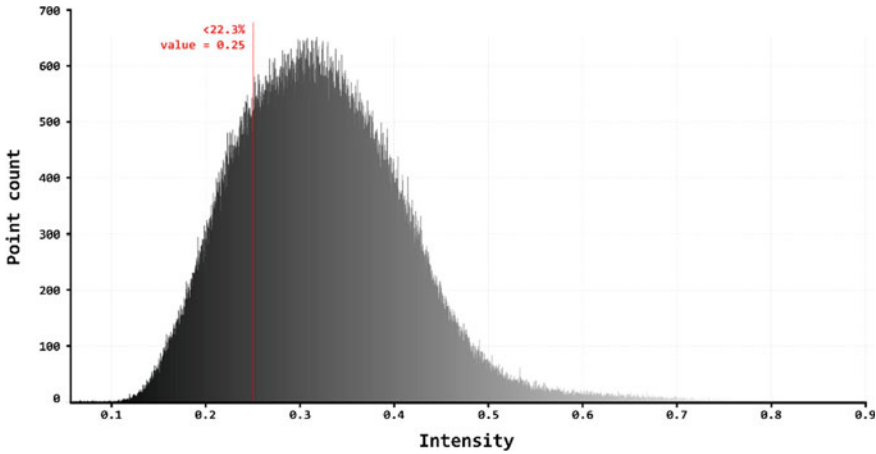
Fig. 4 Greyscale histogram of points and intensities of the pathology sector (1)

Figure 3 displays the segmented area of the pathology (1) dataset enhanced with intensities—in different visualisation modes—where the most affected parts are shown in blue, dark grey, and green colours.

The analysis of the point cloud intensities was carried out considering 3500 classes or intervals. This amount was chosen so that the width of each interval is reduced in order to increase the accuracy of the graph.

Figure 4 shows the histogram of point cloud data intensities for the pathology sector (1).

The analysis yielded the following data:

- 556,171 values (points displaying intensity);
- Mean: 158.91 points (for each intensity value);
- Standard deviation: 213.56 points;
- Point of Interest (PoI): 0.25 intensity value.

The intensity unit is a coefficient, from 0 to 1 (0 to 100%).

Throughout the histogram in Fig. 4, the point arrangement is not symmetrical; i.e. at lower intensities, the point count rate increases more significantly than it decreases at higher intensities. In view of Fig. 3, that is a consequence of the dark areas on the buttress surface. In this way, by mirroring the highest intensities, the ending intensity value of the pathology was established at 0.25 (PoI) for being the symmetry breaking point. Filtering the TLS point cloud data by the intensity PoI, the dataset is split. The remaining 123,498 points with an intensity value lower than 0.25 correspond to the surface deficiency, which constitutes 22.2% of the total number of points in the pathology sector (1).

On the other hand, Fig. 5 displays the segmented area of the reference (2) dataset enhanced with intensities in the monochrome visualisation mode. The reference sector was rectified for comparison by excluding minor pathological zones on it.
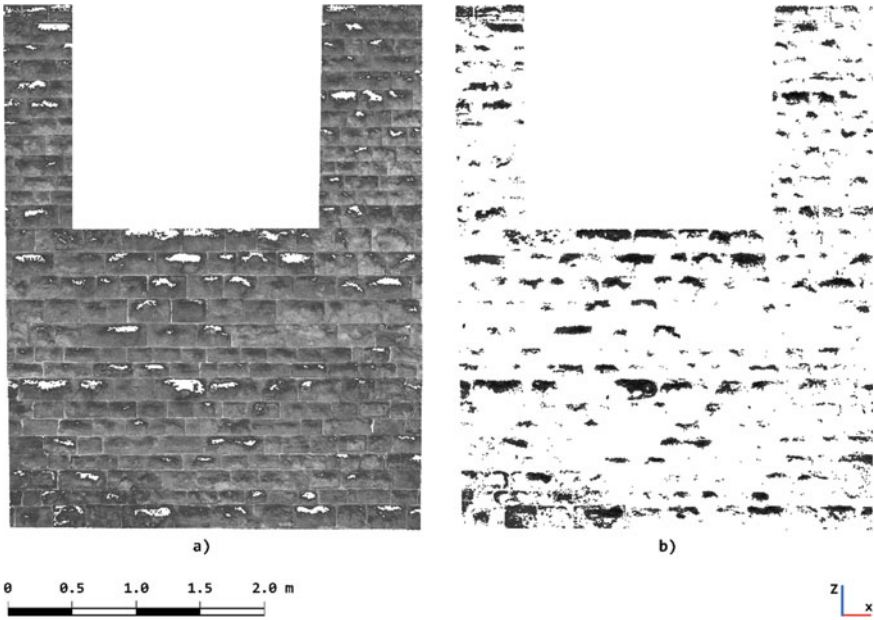
Fig. 5 Segmented reference buttress sector enhanced with intensities, in monochrome: **a** rectified reference sector; **b** minor pathology in the reference sector

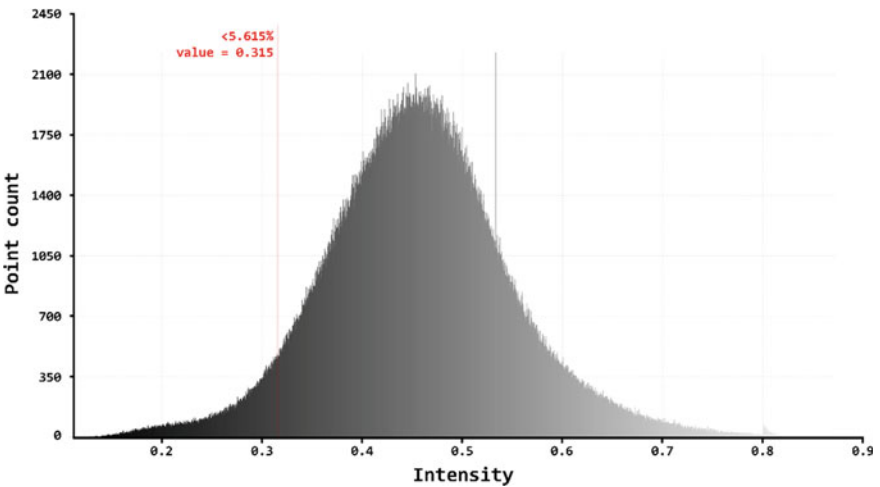Figure 6 shows the histogram of point cloud data intensities for the reference zone (2).

Fig. 6 Greyscale histogram of points and intensities of the reference zone (2)

Also carried out considering 3500 classes, the analysis of the histogram's point cloud intensities yielded the following data:

- 1,645,779 values (points displaying intensity);
- Mean: 470.22 points (for each intensity value);
- Standard deviation: 624.32 points;
- PoI: 0.315 intensity value.

As seen in both histograms, the point distribution is more symmetrical in the reference wall zone against the pathology sector. However, in the region of low-intensity values, the curve symmetry starts at 0.315, thus comprising a small portion of the pathology from 0.1 to 0.315. In view of Fig. 1, the reference wall sector also presents dark zones, but minor. By filtering the point cloud by 0.315 intensity value, the reference point set can be rectified (Fig. 5) and be used as a reference for comparison with the pathology sector.

Similarly to the pathology sector (1), when the point cloud is filtered by the intensity PoI, the remaining 91,475 points correspond to the minor surface deficiency in the reference sector (2) for rectification, which is 5.56% of the total number of points.

Finally, considering the pathology (1) and reference (2) sectors, it is worth analysing the distribution of their data. The coefficient of variation (standard deviation divided by the mean) yields values of 1.344 and 1.328, respectively. This reveals a slightly lower dispersion of the data in (2), which indicates that the points not affected by the pathology prevail.

4.1.2 Bromley House in Beeston

Regarding the residential Bromley House, the colour change throughout the wall constitutes the second sample to be analysed.

Efflorescences are the result of crystallisation of salts on the material surface [19]. This pathology can be easily identified in a photograph and detected using TLS because of the aforementioned changes in laser beam reflection intensity. Figure 7 displays the segmented area of the point cloud enhanced with intensities, where
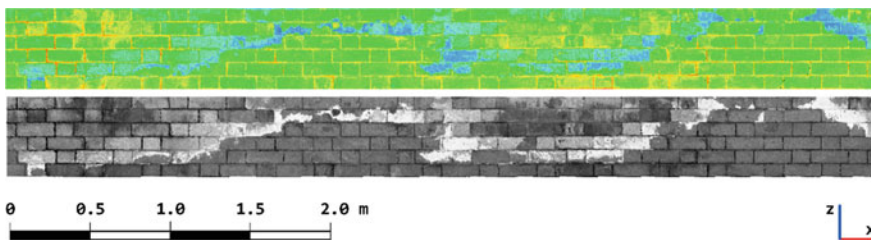

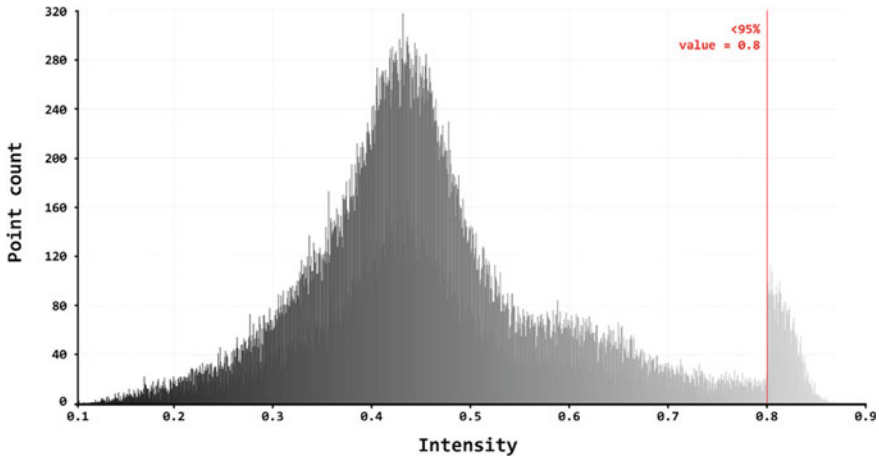**Fig. 7** Segmented wall sector point cloud: top: blue–green–yellow–red; bottom: monochrome

Fig. 8 Greyscale histogram of points and intensities

the more severe efflorescences are shown in blue and light grey to white colours, respectively.

No scan registration diagnostics are provided in this case because the 3D survey consisted of a single scan.

Given the reduced number of points in comparison with the St. Andrew's Church case study, the analysis of the point cloud intensities was carried out considering 2000 classes. Figure 8 shows the histogram of point cloud data intensities.

The analysis yielded the following data:

- 119,772 values (points displaying intensity);
- Mean: 59.89 points (for each intensity value);
- Standard deviation: 65.89 points;
- Image digital level (Digital Number, DN): from 39 to 223 (dark grey to light grey in the histogram);
- Digital level for 0.8 intensity value: 203.

Unlike the more gradual behaviour of the point count rate in the buttress case study, the histogram above (Fig. 8) presents a breaking point in the distribution of points among the intensity intervals in the region of 0.55 intensity value. Considering Figs. 7 and 8 together, 0.55 could represent the starting intensity value of the pathology (efflorescences), which is on the right side of the histogram, by the highest intensities. However, it is the sudden increase in the number of points for the 0.8 intensity value that causes it to become a PoI in the histogram, leaving 5% of points above.

Next, the relationship between the surface pathology, the point cloud intensities, and the DN of the images should be addressed. In the histogram's greyscale range (image DN from 39 to 223), the starting and ending colours are not black and white, respectively. Therefore, that range differs from the full range [0, 255] (256 levels, 8-bit encoding) of the point cloud intensities in Fig. 7 (from black to white), which makes

it necessary to convert the former values into a comprehensive scale. Considering the current scale:

0.77 #highest value of the histogram intensity range [0.1, 0.87]# → 255 (highest DN);

then:

$$0.70 \text{ \#PoIs intensity\#} \rightarrow 231.82 \approx 232,$$

meaning that the DN of the PoI is 232 (starting DN of the remaining 5% points) within the full greyscale range [0, 255].

Scale conversion:

$$232 \div 255 \text{ (highest DN)} \approx 0.91;$$

then:

$$223 \text{ (histograms scale)} \times 0.91 \approx 203,$$

which is the PoI's (0.8 intensity value) DN measured in the histogram.

In view of those results, 5% of the points are within 9% of the intensities, which correspond to the highest values. Therefore, it can be stated that the most affected region of the pathology comprises those DN from 232 to 255 (white). Hence, filtering by intensity value, it is possible to extract that 5% of points (6004) from 0.8 to approximately 0.87 intensity. In this way, the most affected part of the building surface deficiency (0.13 m^2) can be detached from the rest of the sector (the total area is 2.63 m^2). It is also worth quantifying the intensities ranging from 0.55 (value where the efflorescences start) to 0.8 (lowest value of the most affected area). In this case, there are 20,369 points affected, 17% of the total number of points in the original segmented sector. Therefore, the complete pathology represents at least 22% of the entire surface area, approximately 0.58 m^2. The intensity values mentioned above were verified by enquiring the DN of the colour of points in the images, such as the starting and ending value of the ranges, and the PoI. Figure 9 shows the entire pathology subdivided into the affected zone and the most affected area, both filtered by the corresponding intensity values above.

Finally, both case studies should be discussed together. As seen in the results, the arrangement of points of the St. Andrew's Church pathology is gradual, whereas the Bromley House's wall sector presents a clear symmetry breaking point around the 0.55 intensity value and a radical change in the distribution of intensities at 0.8. Besides, the coefficient of variation is 1.10 in the Bromley House wall sector, significantly lower than those in the first case study. By concept, this indicates a lower dispersion of the data; i.e. the distribution of points per intensity interval is more homogeneous. Nevertheless, this means a higher range of intensities corresponding to the pathology; in other words, the pathologies stand out from the reference range of intensities (the rest of the wall sector with no surface deficiency).
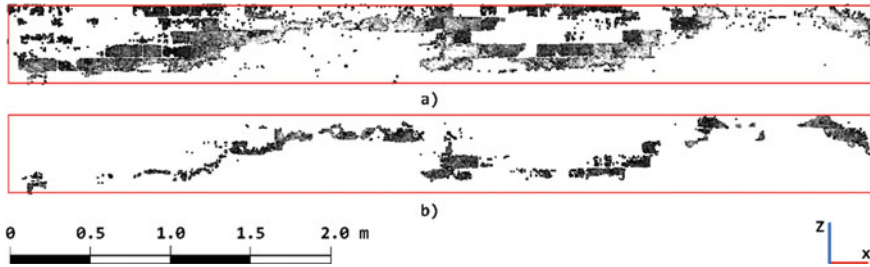
Fig. 9 Filtered efflorescences, in monochrome: **a** intensity value range [0.55, 0.8]; **b** intensity value range [0.8, 0.87]

In addition to the laser beam incidence angle, it is the surface colours that determine the point cloud intensities. In this way, the values of the dark stains on the buttress differ from those of the light grey to white efflorescence on Bromley House. As per the histograms above, the values of the former are consequently lower than those of the latter. Yet, it is demonstrated that TLS, as a remote sensing technique, enables an accurate level of discrimination of surface deficiencies from the non-pathological zones via the analysis of the point cloud intensities.

4.2 Research Limitations

Although the findings of this research derive from a thorough methodology description, and both the qualitative and quantitative analysis of the resulting data, a greater number of samples could provide outcomes of a more robust nature. In relation to the characterisation of pathologies through the laser beam intensity fingerprint, further case studies could lead to a specific analysis of each specific type of deficiency. Besides, the methodology of this research did not take into account the roughness of the surfaces. The produced and filtered intensities were considered to calculate and distinguish between pathologies (most affected points) and reference zones. Finally, some occlusion occurred because of the intrinsic roughness of the masonry blocks of the St. Andrew's Church buttress and the lack of a higher TLS station in the 3D survey. However, the completeness of the dataset has sufficed to draw the above data and the conclusions below.

5 Conclusions

Considering their higher efficiency and accuracy in comparison with traditional methods, previous studies in the field of building surface anomalies have relied on massive data capture technologies to detect and analyse these pathologies. In

this sense, TLS constitutes a particularly interesting option because it allows for recording the intensity of the laser beam reflection onto the objects surveyed. In addition, research has addressed the identification and classification of damaged areas via machine learning and the analysis of TLS radiometric data. However, no research has been found on the analysis of the laser scanning intensity fingerprint of building surface deficiencies. For that purpose, this research analyses the distribution of intensities throughout the geometric data of the selected case studies. In this way, specific intensity values reveal an unusual behaviour in the point count rate among the intensity intervals for a specific type of pathology. This, verified by measuring the digital number (DN) of the deficiencies in the images, leads to filtering the point clouds in order to extract the affected areas. Consequently, the pathologies—and their different degrees—can be quantitatively analysed in the general context of the building component surface. Therefore, based on the analysis of the intensity fingerprint, the TLS remote sensing technique is proven to be useful to record, detect, characterise, and examine specific building surface deficiencies and carry out the conservation status analysis of the buildings surveyed.

Finally, according to one of the conclusions drawn by Dias et al. [6], TLS enables the automation of the visual inspection of façades, and the diagnosis of their degradation condition. Nevertheless, this research reveals that future work on this research topic should be carried out to automate the analysis of the intensity data of building surface deficiencies since the process is at best semi-automatic so far. In this way, a software solution should be sought to fully automate the point cloud filtering and pathology mapping to determine the affected area.

References

1. Antón D, Amaro-Mellado J-L (2021) Engineering graphics for thermal assessment: 3D thermal data visualisation based on infrared thermography, GIS and 3D point cloud processing software. Symmetry (Basel) 13:335. https://doi.org/10.3390/sym13020335
2. Antón D, Medjdoub B, Shrahily R, Moyano J (2018) Accuracy evaluation of the semi-automatic 3D modeling for historical building information models. Int J Archit Heritage 12:790–805. https://doi.org/10.1080/15583058.2017.1415391
3. Antón D, Pineda P, Medjdoub B, Iranzo A (2019) As-built 3D heritage city modelling to support numerical structural analysis: application to the assessment of an archaeological remain. Remote Sens 11:1276. https://doi.org/10.3390/rs11111276

4. Armesto-González J, Riveiro-Rodríguez B, González-Aguilera D, Rivas-Brea MT (2010) Terrestrial laser scanning intensity data applied to damage detection for historical buildings. J Archaeol Sci 37:3037–3047. https://doi.org/10.1016/j.jas.2010.06.031

5. Delgado JMPQ (2021) Case studies of building rehabilitation and design. Springer International Publishing, Cham

6. Dias I, Flores-Colen I, Silva A (2021) Critical analysis about emerging technologies for building's façade inspection. Buildings 11:53. https://doi.org/10.3390/buildings11020053

7. Girardeau-Montaut D (2016) CloudCompare: 3D point cloud and mesh processing software. Open Source Project

8. Google Inc. (2021) Street view. In: What is str. view? https://www.google.com/intl/eng/street view/. Accessed 22 Dec 2021

9. He K, Jia MT, Mei-Fang C (2020) Entropy evaluation method for sandstone uranium reservoir characteristics based on convex hull search. IEEE Access 8:46307–46323. https://doi.org/10.1109/ACCESS.2020.2978153

10. Hichri N, Stefani, De Luca, Veron P (2013) Review of the «As-Built Bim» approaches. Int Arch Photogramm Remote Sens Spat Inf Sci ISPRS Arch XL-5/W1:107–112. https://doi.org/10.5194/isprsarchives-XL-5-W1-107-2013

11. Historic England (1995) Church of St. Andrew's and attached former Sunday school, Non Civil Parish—1270832. In: Listing. https://historicengland.org.uk/listing/the-list/list-entry/1270832. Accessed 6 Aug 2021

12. Historic England (1995) Boundary wall, railings and gates to Church of St Andrew, Non Civil Parish—1247549. In: Listing. https://historicengland.org.uk/listing/the-list/list-entry/1247549. Accessed 21 Dec 2021

13. Historic England (2021) Search the list—find listed buildings, monuments, battlefields and more. In: Listing. https://historicengland.org.uk/listing/the-list/. Accessed 22 Dec 2021

14. Historic England (1987) Church of St John the Baptist, non civil Parish—1263823. In: Listing. https://historicengland.org.uk/listing/the-list/list-entry/1263823. Accessed 7 Dec 2021

15. Historic England (1987) Village cross, non civil Parish—1263870. In: Listing. https://historicengland.org.uk/listing/the-list/list-entry/1263870. Accessed 21 Dec 2021

16. Kim M, Sohn H, Chang C-C (2015) Localization and quantification of concrete spalling defects using terrestrial laser scanning. J Comput Civ Eng 29:04014086. https://doi.org/10.1061/(ASCE)CP.1943-5487.0000415

17. Leica Geosystems (2012) Leica ScanStation P20—industry's best performing ultra-high speed scanner. In: Scanners. http://w3.leica-geosystems.com/downloads123/hds/hds/ScanStation_P20/brochures-datasheet/Leica_ScanStation_P20_DAT_us.pdf. Accessed 15 June 2021

18. Leica Geosystems (2019) Leica cyclone—3D point cloud processing software

19. Lerma C, Mas Á, Gil E et al (2014) Pathology of building materials in historic buildings. Relationship between laboratory testing and infrared thermography. Mater Constr 64:e009. https://doi.org/10.3989/mc.2013.06612

20. Lezzerini M, Antonelli F, Columbu S et al (2016) Cultural heritage documentation and conservation: three-dimensional (3D) laser scanning and geographical information system (GIS) techniques for thematic mapping of facade stonework of St. Nicholas Church (Pisa, Italy). Int J Archit Heritage 10:9–19. https://doi.org/10.1080/15583058.2014.924605

21. Mallafrè Balsells C, López Besora JM, Costa Jover A, Coll Pla S (2021) Register of dry stone domes. simplified method for point clouds. Nexus Netw J 23:493–506. https://doi.org/10.1007/S00004-020-00533-W/FIGURES/8

22. Masiero A, Costantino D (2019) TLS for detecting small damages on a building façade. Int Arch Photogramm Remote Sens Spat Inf Sci XLII-2/W11:831–836. https://doi.org/10.5194/isprs-archives-XLII-2-W11-831-2019

23. Sitzia F, Lisci C, Mirão J (2021) Building pathology and environment: weathering and decay of stone construction materials subjected to a Csa mediterranean climate laboratory simulation. Constr Build Mater 300:124311. https://doi.org/10.1016/j.conbuildmat.2021.124311

24. Smith M, Gorse C (2021) Building surveyor's pocket book, 1st edn. Routledge, Abingdon, Oxon; New York, NY

25. St. Andrew's with Castle Gate United Reformed Church (2021) St. Andrew's with castle gate United Reformed Church. In: St. Andrew's with castle gate United Reform. Church—living God's love through faith action. https://standrewswithcastlegate.org.uk/. Accessed 6 Aug 2021
26. Suchocki C, Błaszczak-Bąk W, Janicka J, Dumalski A (2021) Detection of defects in building walls using modified OptD method for down-sampling of point clouds. Build Res Inf 49:197–215. https://doi.org/10.1080/09613218.2020.1729687
27. The Southwell and Nottingham Church History Project (2021) Beeston St. John the Baptist. In: Southwell Nottingham Church historty project. https://southwellchurches.nottingham.ac.uk/beeston/hintro.php. Accessed 7 Dec 2021
28. Valero E, Forster A, Bosché F et al (2019) Automated defect detection and classification in ashlar masonry walls using machine learning. Autom Constr 106:102846. https://doi.org/10.1016/j.autcon.2019.102846